Automated CT Image Reconstruction of Zygomatic Fractures for Preoperative Planning and Navigation in Reduction Surgery

Zahra Montazeriani (PhD)[1,2], Pezhman Pasyar (PhD)[1,2], Mohammad Bayat (MD)[3,4], Hossein Arabalibeik (PhD)[1,2], Naghmeh Bahrami (PhD)[4,5], Mehrnoush Momeni Roochi (MD)[3], Alireza Ahmadian (PhD)[1,2]*

[1]Department of Medical Physics and Biomedical Engineering, Tehran University of Medical Sciences, Tehran, Iran
[2]Research Centre for Biomedical Technologies and Robotics (RCBTR), Advanced Medical Technologies and Equipment Institute (AMTEI), Tehran University of Medical Sciences, Tehran, Iran
[3]Department of Oral and Maxillofacial Surgery, School of Dentistry, Tehran University of Medical Sciences, Tehran, Iran
[4]Craniomaxillofacial Research Center, Shariati Hospital, Tehran University of Medical Sciences, Tehran, Iran
[5]Department of Tissue Engineering and Applied Cellular Sciences, School of Advanced Technologies in Medicine, Tehran University of Medical Sciences, Tehran, Iran

ABSTRACT

Background: The Zygomaticomaxillary Complex (ZMC) is essential for facial structure, function, and aesthetics. Due to its prominent anatomical position, the zygoma is highly prone to fractures. Accurate reconstruction of Computed Tomography (CT) images in such cases is crucial for fracture reduction, fragment repositioning, and the design of patient-specific implants. However, reconstructing defective regions with precision is often time-consuming and requires close collaboration between surgeons and medical modeling experts.

Objective: This study aimed to develop an automated deep learning-based method for CT image reconstruction of zygomatic fractures to support surgical planning and navigation.

Material and Methods: In this computational experimental study, an automated deep learning approach was implemented for CT image reconstruction of zygomatic fractures, using a modified U-Net architecture with dilated convolution blocks. The method was evaluated quantitatively using several metrics, including the Dice Similarity Coefficient (DSC), Jaccard Index, Precision, Recall, Specificity, Hausdorff Distance, and surface analysis.

Results: The proposed model demonstrated high accuracy, achieving DSC values of 0.98 and 0.96 for the border and surface regions of the zygoma, respectively, indicating its strong capability in reconstructing missing regions with high fidelity.

Conclusion: This automated method provides a reliable and effective solution for reconstructing zygomatic defects, offering valuable support for preoperative planning and intraoperative navigation in zygoma reduction surgeries.

Keywords

Deep Learning; Image Processing; Zygomatic Fractures; Surgical Navigation Systems

Introduction

The Zygomaticomaxillary Complex (ZMC) plays a crucial role in facial structure, function, and aesthetics [1]. ZMC fractures are among the most common midface injuries, accounting for approximately 40% of cases, second only to nasal fractures [2]. Due to

*Corresponding author:
Alireza Ahmadian
Department of Medical Physics and Biomedical Engineering, Tehran University of Medical Sciences, Tehran, Iran
E-mail:
ahmadian@tums.ac.ir

Received: 26 April 2025
Accepted: 29 June 2025

its prominent anatomical position, the zygoma is particularly susceptible to fractures, and the complex three-dimensional structure of the ZMC makes surgical restoration especially challenging [3].

Several classification systems have been proposed for zygomatic fractures to assist in diagnosis and surgical planning [4-6]. Among them, Markus Zingg's classification is widely used; in this system, type-B fractures involve all four components of the zygomatic bone's tetrapod structure, leading to complete separation from the skull [4]. The primary objective of reduction surgery is to restore facial symmetry and function through the precise repositioning of the fractured zygoma to its original anatomical position. When performed early, proper reduction surgery improves outcomes, shortens recovery time, and reduces the need for additional surgeries, specialized implants, and unnecessary costs.

Preoperative planning is critical in such cases, as it allows for the creation of a reconstructed skull map to guide the precise repositioning of the zygoma during surgery [7]. Various techniques have been developed for reconstructing facial defects, including atlas-based approaches [8], mirroring methods [9], and Statistical Shape Models (SSM) [10]. However, these techniques are often manual or semi-automatic, requiring close collaboration between surgeons and Computer-Aided Design (CAD) specialists. As a result, they can be time-consuming, labor-intensive, and costly [11].

Recently, deep learning techniques have gained significant attention in the medical field for tasks such as segmentation [12], classification [13], denoising [14], and reconstruction [15]. In this context, defect reconstruction and implant design can be formulated as a shape completion problem. Several methods have been proposed for virtual cranial reconstruction to support preoperative planning. These approaches are generally classified into five categories:

Mirroring-based approaches reconstruct the defective region by reflecting the healthy side of the cranium onto the damaged area. This method is relatively simple and uses the patient's anatomy as a template. However, it often requires significant user interaction to produce a well-fitted model. These techniques depend on cranial symmetry by identifying the midface plane and mirroring the healthy side onto the defect, followed by manual adjustments. In practice, human faces are rarely perfectly symmetrical [16], which makes accurate midplane determination challenging. Moreover, these methods are limited to the restoration of unilateral defects.

Template-based techniques use pre-existing models of healthy skulls, either as a single template or as part of an atlas. In atlas-based methods, the patient's model is aligned with the template using anatomical landmarks, followed by additional adjustments for a proper fit [17, 18]. While this approach can restore defects of any size or location, it requires substantial user interaction, is time-consuming, and depends heavily on accurate landmark identification.

Slice-based methods reconstruct the three-dimensional shape by sequentially restoring individual two-dimensional slices of the defective structure. In these techniques, closed curves are fitted to the bone contours on each 2D CT or MRI slice. The missing region is then reconstructed by aligning these curves to ensure a smooth transition between the defective and healthy areas [19, 20]. Some approaches use Recurrent Neural Networks (RNNs) to incorporate information from adjacent slices, improving continuity in the reconstructed region. However, the lack of information within the missing area can limit reconstruction accuracy. Additionally, the extracted curves must be stacked to fully reconstruct the skull.

Point cloud or mesh-based techniques approach shape completion as a Point Cloud (PC) reconstruction task, using unstructured PC data to restore missing regions [21]. The

completed point cloud can then be voxelized to create a volumetric representation. These methods offer computational efficiency due to the sparse nature of point clouds. However, their accuracy still falls short of volumetric-based approaches.

Voxel-based methods work with volumetric data, often obtained by voxelizing point clouds or mesh representations. These techniques restore the missing structure by completing the voxel grid. Among automated methods, Convolutional Neural Networks (CNNs) have achieved the highest reconstruction accuracy [22], though they require higher computational resources. The reconstructed voxel grid can then be converted into meshes for applications such as 3D printing.

While many of these methods offer promising results, recent research [23-29] has increasingly focused on automatic cranium reconstruction for implant design.

Some approaches first reconstruct the complete skull from the defective model and then generate the implant using subtraction algorithms, while others directly predict the implant shape. Li et al. [23] proposed a three-step implant generation scheme based on autoencoders, predicting cranial implants in a coarse-to-fine manner. Resmi et al. [24] combined a 3D U-Net with transformers to reconstruct cranial implants from low-resolution images. Matzkin et al. [25] reconstructed both the implant and the complete skull using U-Net models and further improved their method by incorporating a skull template as a shape prior [26]. To address the lack of defective skull datasets, they augmented their data using spherical and cubic shapes to simulate artifacts.

Other studies have focused on automatic data augmentation through registration. Ellis et al. [27] used a residual U-Net to enhance reconstruction performance, though at the cost of higher computation time. Similarly, Wodzinski et al. [28] employed a residual U-Net and augmented their training set by combining multiple datasets through registration.

Beyond cranial implants, deep learning has also been applied to other facial reconstructions. Xiong et al. [29] developed a Generative Adversarial Network (GAN)-based model for reconstructing 2D images of midface defects, while Fang et al. [11] used a residual U-Net with a dilated bottleneck to reconstruct mandibular defects.

In this study, we present an automatic deep learning-based method for reconstructing zygomatic CT images using a modified U-Net architecture. We also introduce a wrapping technique to increase input resolution, reduce the need for large datasets or extensive augmentation, and simplify both the model and training process. Additionally, we demonstrate the clinical potential of our approach by applying it to the reduction of a 3D fractured phantom using a surgical navigation system.

Material and Methods

This computational experimental study presents an automated deep learning-based approach for CT image reconstruction of zygomatic fractures. The method employs a modified U-Net architecture enhanced with dilated convolution blocks to improve feature extraction and reconstruction accuracy. The model's performance is quantitatively evaluated using standard metrics. Its practical feasibility is also demonstrated through a navigated reduction surgery performed on a 3D-printed phantom model.

Dataset Collection

All data were obtained from the Parsiss dataset (Parseh Co., Tehran, Iran). From a pool of 2,000 CT scans, 200 images of healthy skulls were selected based on the following inclusion criteria: age between 10 and 60 years, slice thickness of ≤1 mm, full coverage of the ZMC region, and a complete skull. Scans with midface deformities or dental artifacts were excluded. The dataset includes varying in-plane resolutions and slice spacings.

Preprocessing

Normal CT images were imported into Mimics Research 21.0 (Materialise Co., Leuven, Belgium) to generate 3D models of healthy skulls. Bone and dental structures were extracted using thresholding based on Hounsfield Units (HU), followed by region growing. The mandible and spinal components were then removed.

To improve the training process, the 3D skull models were aligned with a reference model using the Iterative Closest Point (ICP) algorithm. This step minimized image-related inconsistencies, such as rotation and translation, enabling the deep neural network to better capture skull shape variations and detect defects [19].

Further refinements included smoothing and mesh reduction to simplify the data while preserving critical anatomical features. Finally, a wrapping technique was applied to seal unnecessary cavities, resulting in optimized STL (STereoLithography) models suitable for advanced tasks, such as image reconstruction and implant design.

Synthetic Training Data Generation

Training a neural network for fracture image reconstruction requires paired datasets containing both fractured and non-fractured images. To create such data, artificial fractures were generated on 3D models of healthy skulls.

Given the high anatomical similarity among healthy skulls, reducing size variability can improve model training [30]. Therefore, all models were rescaled to a standardized size of 256×256×256 voxels, with scaling factors stored for later restoration to the original dimensions. The zygomatic bone region was then isolated by introducing a synthetic defect. This was achieved by intersecting a spherical defect with the skull model [31]. The center of the sphere was randomly positioned within a 10 mm radius from a manually selected landmark marking the outermost point of the zygoma. The defect size was defined by assigning a random radius between 20 mm and 25 mm (Figure 1).

For each of the 200 initial models, three datasets were generated: the complete skull, the fractured zygomatic skull (defective skull), and the corresponding zygomatic implant. All volumetric models were voxelized and stored as binary voxel grids with dimensions of 256×256×256. The dataset was then split into training (160 samples), validation (20 samples), and testing (20 samples) sets for model development and evaluation.

Model Architecture

We employed a Residual U-Net–based convolutional neural network for image reconstruction. Given the relative symmetry of the skull, incorporating a large receptive field enables the network to capture global structural features more effectively, thereby enhancing reconstruction accuracy.

We propose a novel architecture that

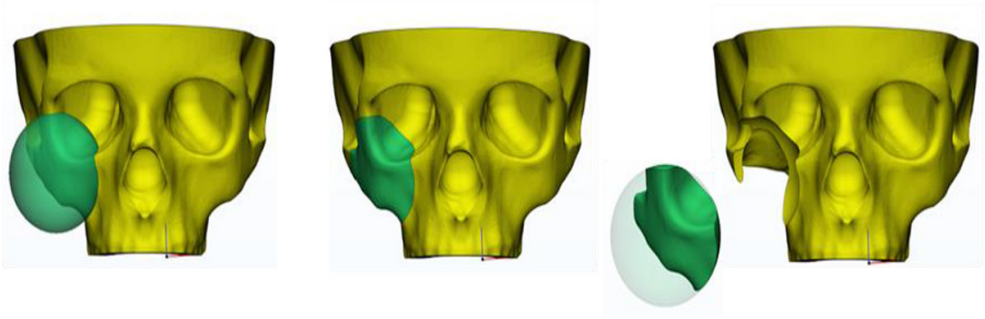

Figure 1: Example of an artificially generated zygomatic defect in a healthy skull model.

integrates dilated convolution blocks into the U-Net's skip connections. The dilation factor progressively decreases in deeper layers to refine feature extraction (Figure 2). The encoder consists of five layers, each containing convolutional and residual blocks, followed by Group Normalization, and Leaky ReLU activation. The number of channels doubles at each successive layer. In the decoder, the output from the corresponding encoder layer (after dilated convolution) is concatenated with the output of the previous decoder layer to serve as input. A final block with Sigmoid activation produces the reconstructed image. Each dilated block includes convolutional layers followed by Group Normalization and a skip connection path to preserve feature continuity.

Training and Evaluation

The model was implemented in PyTorch [32] and optimized using the Adam optimizer [33], with an initial learning rate of 0.003 and a decay rate of 0.99. All experiments were conducted on a Windows-based system equipped with an Intel CPU (2.24 GHz) and an NVIDIA RTX 4090 GPU (24 GB VRAM).

To improve model generalization and reduce overfitting, random data augmentations were applied during training. These included scaling (0.99 to 1.1), translation (±5 pixels), and rotation (±5 degrees).

To achieve complete skull reconstruction, the loss function combines both global and local Dice Similarity Coefficient (DSC). The global Dice term preserves healthy skull regions, while the local Dice term focuses on reconstructing missing areas. For implant reconstruction, the loss function emphasizes the Border Dice Similarity Coefficient (BDSC), which measures reconstruction accuracy near the junction between the implant and the damaged bone. Given the importance of accurately restoring external fracture surfaces for precise surgical planning, we employed the Surface Dice Similarity Coefficient (SDSC) as the local Dice term. The SDSC is calculated within a defined distance from the implant surface to

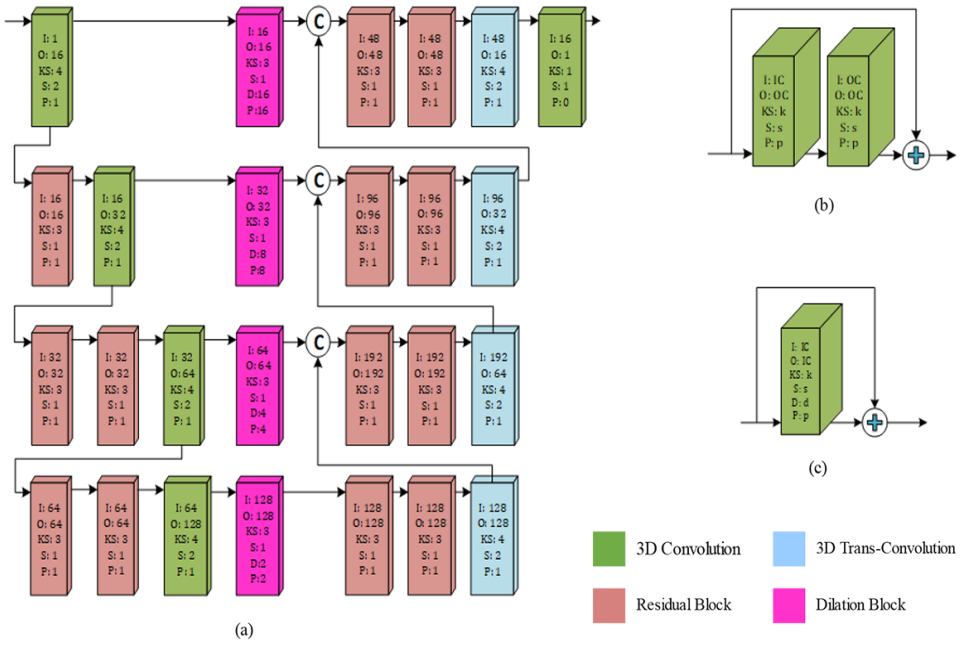

Figure 2: Overview of the proposed network architecture and its components. (**a**) Proposed Dilated U-Net architecture; (**b**) Residual Block; (**c**) Dilation Block. (I: Input channels, O: Output channels, KS: Kernel Size, S: Stride, P: Padding, D: Dilation rate).

evaluate surface reconstruction. The BDSC is critical for assessing border accuracy, essential for implant design, while the SDSC evaluates surface restoration, particularly relevant for correcting enophthalmos and restoring facial symmetry during zygomatic reduction. The total loss function is defined as a weighted sum of the global and local Dice terms, with a weighting ratio of 3:7.

The model's performance was evaluated using multiple metrics, including Hausdorff Distance [34], surface analysis [10], F1-Score, Jaccard Index, Precision, Specificity, and Recall [11].

Post-processing and Preoperative Planning

To remove spurious voxels from the reconstructed skull, a morphological opening operation was applied, effectively eliminating weakly connected or isolated voxels. The reconstructed skull was then up-sampled and rescaled to its original dimensions.

For preoperative planning, the fractured segment was realigned using the reconstructed model through the ICP registration algorithm. This model served as a surgical guide, enabling precise zygoma reduction based on manually selected anatomical landmarks.

Intraoperative Tracking and Reduction

Intraoperative navigation was conducted using the Parsiss navigation system (Parseh Co., Tehran, Iran). Navigators were securely attached to both the head and the fractured segment to enable real-time tracking of the fractured part relative to the defective skull. Manual landmark selection was performed to register and align the 3D models within the navigation system. Once proper alignment was achieved, the reduction was completed by fixing the zygoma to the skull using titanium plates at two or three points.

To evaluate the navigated reduction procedure, a defective skull was designed and 3D-printed by PTD (Pishgaman Teb Digital Co., Tehran, Iran). After fixing the fractured segment to the skull, a CT scan of the phantom was performed, and the results were assessed through surface analysis. Figure 3 shows the navigated reduction process on the phantom.

For clinical application, the fractured segment and its surrounding area are removed from the CT scan using a spherical mask before reconstruction. Applying a spherical

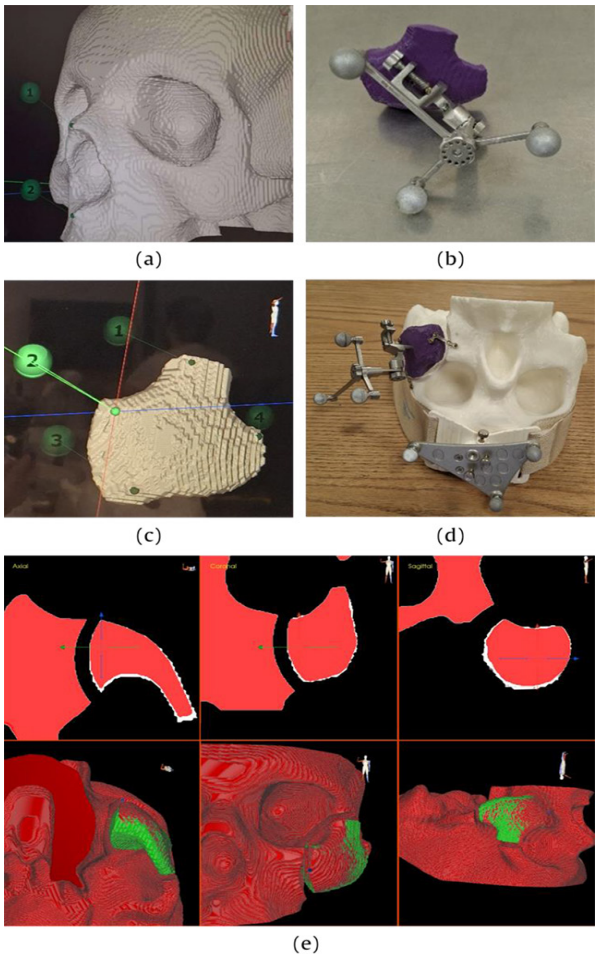

Figure 3: Navigated reduction procedure of a fractured zygoma using a 3D-printed phantom. (**a**) Landmark selection on the defective skull, (**b**) Attachment of the navigator to the fractured segment, (**c**) Landmark selection on the fractured zygoma, (**d**) Final outcome showing the reduced and fixed fracture, and (**e**) Navigation-guided reduction process using the Parsiss navigation system software.

defect in both the simulation and reconstruction phases ensures methodological consistency and preserves the robustness of the model's performance.

Results

The quantitative evaluation of defect reconstruction is summarized in Table 1, based on the F1-Score, BDSC, SDSC, and the 95th percentile of the Border and Surface Hausdorff Distances (BHD95 and SHD95). The BDSC measures Dice similarity within a specified Euclidean distance from the defect border, while the SDSC quantifies Dice similarity around the defect surface within a defined distance.

The performance of the model on the test set (20 cases) is presented in Table 2, reporting Jaccard, Recall, Precision, and Specificity, all evaluated within the defect surface region.

The navigated zygoma reduction procedure was performed on a 3D-printed phantom. CT images of the phantom were acquired using a GE (General Electric Co., New York, United States) CT scanner with a slice thickness of 1 mm. Surface analysis between the reduced and reference zygoma, conducted using Geomagic (3D Systems Co., South Carolina, United States) software, is shown in Figure 4. The mean surface error was **0.6929 mm** (standard deviation: **1.137 mm**), with a Root Mean Square (RMS) error of **1.3315 mm**. Table 3 summarizes and compares previous reconstruction algorithms, focusing on reconstruction approach, model complexity, dataset characteristics, reconstructed regions, and other relevant factors.

Discussion

Virtual reconstruction of defective skulls plays a crucial role in guiding bone fracture repositioning and implant design. While much of the existing research has focused on cranioplasty, midface reconstruction remains more challenging due to the intricate anatomy and complex surfaces of the midfacial bones. Consequently, relatively few studies have addressed midface or mandibular reconstruction.

Early studies in cranial reconstruction primarily employed autoencoders for implant generation. For example, study [23] utilized a cascade autoencoder comprising 82 million parameters, achieving a DSC of 0.80 with an input resolution of 128×128×64. Later, U-Net architectures were adopted to improve performance. Studies [25, 26] increased the input

Table 1: Quantitative performance metrics obtained during model training.

	F1-Score	BDCS	SDCS	BHD95[mm]	SHD95[mm]
Train	0.9994	0.9882	0.9801	0.854	0.854
Evaluation	0.9987	0.9760	0.9518	1.496	1.938

BDCS: Border Dice Similarity Coefficient, SDCS: Surface Dice Similarity Coefficient, BHD95: 95th percentile of Border Hausdorff Distance, SHD95: 95th percentile of Surface Hausdorff Distance.

Table 2: Quantitative results for the test set. Jaccard index, Recall, Precision, and Specificity are evaluated within the defect surface region.

	F1-Score	BDCS	SDCS	BHD95[mm]	SHD95[mm]	Jaccard	Recall	Precision	Specificity
Mean	0.999	0.984	0.963	1.658	2.129	0.928	0.967	0.959	0.999
Std	6.57×10^{-4}	0.003	0.009	0.549	0.459	0.016	0.011	0.019	0.47×10^{-4}

BDCS: Border Dice Similarity Coefficient, SDCS: Surface Dice Similarity Coefficient, BHD95: 95th percentile of Border Hausdorff Distance, SHD95: 95th percentile of Surface Hausdorff Distance.

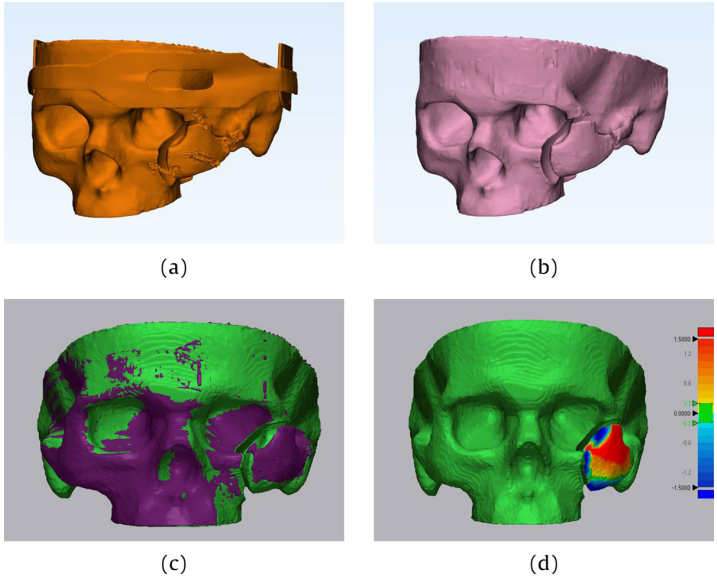

Figure 4: Computed Tomography (CT) images and surface analysis of the phantom. (**a**) CT model showing the reduced and fixed zygoma. (**b**) Post-processed model prepared for surface analysis after removing the headband and splints. (**c**) Alignment of the reduced model (purple) with the reference model (green). (**d**) Surface distance map displaying deviations between the reduced and reference models, measured in millimeters.

Table 3: Summary and comparison of reconstruction algorithms

Study	Area	Dataset	Architecture	Input Dim	Output	Results	Hardware	#Param
[23]	Crania	200 healthy	Cascade Autoencoder	128×128×64	Implant	DSC=0.80 HD=5.4 mm RE=0.15	GTX 1070 Ti 8G RAM	82.72 M
[24]	Crania	100 healthy	U-Net +Transformer	64×64×64	Implant	DSC=0.79	V100 and T4 GPUs and 51GB RAM	-
[25]	Crania	67 healthy	U-Net	304×304×224	Implant	DSC=0.90 HD=4.47 mm	TITAN Xp 12G RAM	-
[26]	Crania	200 healthy 10 patients	U-Net Shape prior	304×304×224	Implant	DSC=0.84 HD=6.37 mm	TITAN Xp 12G RAM	5.19 M
[27]	Crania	9913	Res U-Net	176×224×144	Skull	DSC=0.94 HD=3.59 mm	2×V100 2×32G RAM	68.56 M
[28]	Crania	100,000	Res U-Net	240×200×240	Implant	DSC=0.91 HD95=1.53 mm	8×V100 8×32 GB RAM 2×RTX 3090 2×24 GB RAM	12.7 M
[29]	Midface	518 healthy 17 patients	GAN	512×512	Skull	Cosine=0.96	4×Tesla Titan 4×32 GB RAM	-
[11]	Mandible	80 healthy	Res U-Net Dilation	64×64×64	Mandible Implant	DSC_mandible=0.98 DSC_implant=0.80	-	-

DSC: Dice Similarity Coefficient, HD: Hausdorff Distance, RE: Reconstruction Error, GAN: Generative Adversarial Network, GPU: Graphics Processing Unit, RAM: Random Access Memory, GB: Gigabyte, GTX: Giga Texel shader eXtreme, M: million.

resolution to 304×304×224 and achieved a DSC of 0.90. Further advancements involved Residual U-Net architectures. Study [27] introduced a Residual U-Net with 68 million parameters and implemented augmentation via registration, achieving a DSC of 0.94 using inputs of size 176×224×144. Study [28] extended this approach by training a Residual U-Net on 100,000 images from multiple datasets, reporting a DSC of 0.91 for implant design. However, all these studies focused exclusively on cranial reconstruction and emphasized the greater complexity of midface reconstruction.

In an effort to simplify models for lower-resolution images, study [24] proposed a hybrid architecture combining a 3D U-Net with transformers; however, the model did not exceed a DSC of 0.79 for an input size of 64×64×64.

Regarding midface reconstruction, study [29] applied a GAN-based network for reconstructing 2D images of midface defects, achieving a cosine similarity of 0.96. Study [11] proposed a Residual U-Net incorporating dilation blocks in the bottleneck to reconstruct mandibular defects, reaching a DSC of 0.98 for the mandible and 0.80 for implants. However, they noted that increasing the input size beyond 64×64×64 reduced reconstruction accuracy, limiting the model's applicability for high-resolution outputs.

In this study, we developed a Residual U-Net architecture enhanced with dilation blocks in the skip connections for reconstructing zygomatic defects. The inclusion of dilation layers enabled the network to capture a broader anatomical context, leveraging contralateral symmetry to improve reconstruction performance. Furthermore, we employed a wrapping method to exclude irrelevant structures, such as the nasal inner wall, thereby allowing us to increase the input resolution to 256×256×256. This higher resolution proved effective for both defect reconstruction and implant design, addressing a key limitation of previous approaches in midface reconstruction.

Our model was trained using random transformations at each step on a dataset of 200 virtually fractured healthy skulls. The architecture, consisting of approximately 12 million parameters, was trained on an NVIDIA RTX 4090 GPU (24 GB VRAM). The results demonstrated high reconstruction accuracy, achieving a DSC of 0.98 in the border region and 0.96 in the surface region of the zygoma.

The dataset employed in this study included CT scans from 200 healthy individuals, comprising both male and female subjects aged 10 to 60 years. Future improvements could be achieved by expanding the dataset through additional data augmentation techniques or integrating external datasets. Incorporating real patient defect cases would also enhance the model's clinical relevance. Furthermore, stratifying the dataset based on sex-specific characteristics (e.g., male vs. female skulls) may improve reconstruction performance, given known anthropometric differences. Additional studies are warranted to evaluate the model's robustness in more complex scenarios, such as bilateral defects or reconstructions involving other midface regions, to expand its clinical applicability. Moreover, the impact of intraoperative navigation errors (including landmark selection accuracy, registration precision, and fixation stability) should be systematically assessed, as these factors can significantly affect the surgical outcome in zygomatic reduction procedures.

Conclusion

This study presented an automated 3D reconstruction method for zygomatic fractures in CT images using an enhanced Residual U-Net architecture with integrated dilation blocks. The proposed model demonstrated high accuracy in reconstructing defective skull regions while preserving a high input resolution, addressing the challenges of midface reconstruction. The results suggest that this approach can provide valuable preoperative guidance for navigated zygoma reduction surgeries. Future research should focus on expanding the dataset,

improving resolution, and validating the method on real clinical cases to further establish its clinical utility and generalizability.

Acknowledgment

We thank our colleagues from and Advanced Medical Technologies and Equipment Institute (AMTEI) who provided insight and expertise that greatly assisted the research.

Authors' Contribution

Z. Montazeriani developed the methodology and algorithms, conducted the experiments and simulations, and analyzed the data and results. P. Pasyar contributed to conceptualization, algorithm development, result interpretation, and manuscript preparation. M. Bayat designed the surgical strategy, performed preoperative planning, developed the 3D phantom, and conducted the phantom surgeries. H. Arabalibeik assisted in conceptualization, algorithm design, and result analysis. N. Bahrami supported the initial study design, preoperative planning, and surgical coordination. M. Momeni Roochi participated in surgical planning. A. Ahmadian, the corresponding author, contributed to conceptualization, data collection, surgical equipment provision, and navigation planning. All authors reviewed and approved the final manuscript.

Ethical Approval

This study used anonymized data and involved no direct human intervention. It was approved by the Ethics Committee of Tehran University of Medical Sciences under code IR.TUMS.MEDICINE.REC.1399.1096.

Informed Consent

No informed consent is required as the study does not involve human subjects.

Funding

This study was supported by Tehran University of Medical Sciences (TUMS) [grant number 50808-101-3-99].

Conflict of Interest

None

References

1. Ho JPTF, Schreurs R, Aydi S, Rezai R, Maal TJJ, Van Wijk AJ, et al. Natural variation of the zygomaticomaxillary complex symmetry in normal individuals. *J Craniomaxillofac Surg.* 2017;**45**(12):1927-33. doi: 10.1016/j.jcms.2017.09.017. PubMed PMID: 29046241.
2. Farber SJ, Nguyen DC, Skolnick GB, Woo AS, Patel KB. Current Management of Zygomaticomaxillary Complex Fractures: A Multidisciplinary Survey and Literature Review. *Craniomaxillofac Trauma Reconstr.* 2016;**9**(4):313-22. doi: 10.1055/s-0036-1592093. PubMed PMID: 27833710. PubMed PMCID: PMC5101115.
3. Meslemani D, Kellman RM. Zygomaticomaxillary complex fractures. *Arch Facial Plast Surg.* 2012;**14**(1):62-6. doi: 10.1001/archfacial.2011.1415. PubMed PMID: 22250270.
4. Zingg M, Laedrach K, Chen J, Chowdhury K, Vuillemin T, Sutter F, Raveh J. Classification and treatment of zygomatic fractures: a review of 1,025 cases. *J Oral Maxillofac Surg.* 1992;**50**(8):778-90. doi: 10.1016/0278-2391(92)90266-3. PubMed PMID: 1634968.
5. Kristensen S, Tveteråas K. Zygomatic fractures: classification and complications. *Clin Otolaryngol Allied Sci.* 1986;**11**(3):123-9. doi: 10.1111/j.1365-2273.1986.tb00117.x. PubMed PMID: 3731507.
6. Rowe NL, Killey HC. Fractures of the facial skeleton. 2nd ed. Scotland: Edinburgh, Livingstone; 1968.
7. Ogino A, Onishi K, Maruyama Y. Intraoperative repositioning assessment using navigation system in zygomatic fracture. *J Craniofac Surg.* 2009;**20**(4):1061-5. doi: 10.1097/SCS.0b013e3181abb2e8. PubMed PMID: 19553855.
8. Metzger MC, Bittermann G, Dannenberg L, Schmelzeisen R, Gellrich NC, Hohlweg-Majert B, Scheifele C. Design and development of a virtual anatomic atlas of the human skull for automatic segmentation in computer-assisted surgery, preoperative planning, and navigation. *Int J Comput Assist Radiol Surg.* 2013;**8**(5):691-702. doi: 10.1007/s11548-013-0818-6. PubMed PMID: 23417709.
9. Feng F, Wang H, Guan X, Tian W, Jing W, Long

J, et al. Mirror imaging and preshaped titanium plates in the treatment of unilateral malar and zygomatic arch fractures. *Oral Surg Oral Med Oral Pathol Oral Radiol Endod*. 2011;**112**(2):188-94. doi: 10.1016/j.tripleo.2010.10.014. PubMed PMID: 21216634.

10. Fuessinger MA, Schwarz S, Neubauer J, Cornelius CP, Gass M, Poxleitner P, et al. Virtual reconstruction of bilateral midfacial defects by using statistical shape modeling. *J Craniomaxillofac Surg*. 2019;**47**(7):1054-9. doi: 10.1016/j.jcms.2019.03.027. PubMed PMID: 30982558.
11. Fang Z, Liu D, Wu Y. Implant model generation method for mandibular defect based on improved 3D unet. *Applied Sciences*. 2023;**13**(8):4741. doi: 10.3390/app13084741.
12. Rayed ME, Islam SS, Niha SI, Jim JR, Kabir MM, Mridha MF. Deep learning for medical image segmentation: State-of-the-art advancements and challenges. *Inform Med Unlocked.* 2024;**47**:101504. doi: 10.1016/j.imu.2024.101504.
13. Pasyar P, Mahmoudi T, Kouzehkanan SZ, Ahmadian A, Arabalibeik H, Soltanian N, Radmard AR. Hybrid classification of diffuse liver diseases in ultrasound images using deep convolutional neural networks. *Inform Med Unlocked.* 2021;**22**:100496. doi: 10.1016/j.imu.2020.100496.
14. Nazir N, Sarwar A, Saini BS. Recent developments in denoising medical images using deep learning: An overview of models, techniques, and challenges. *Micron.* 2024;**180**:103615. doi: 10.1016/j.micron.2024.103615. PubMed PMID: 38471391.
15. Ahishakiye E, Bastiaan Van Gijzen M, Tumwiine J, Wario R, Obungoloch J. A survey on deep learning in medical image reconstruction. *Intelligent Medicine.* 2021;**1**(03):118-27. doi: 10.1016/j.imed.2021.03.003.
16. Shah SM, Joshi MR. An assessment of asymmetry in the normal craniofacial complex. *Angle Orthod.* 1978;**48**(2):141-8. doi: 10.1043/0003-3219(1978)048<0141:AAOAIT>2.0.CO;2. PubMed PMID: 277077.
17. Marreiros FM, Heuzé Y, Verius M, Unterhofer C, Freysinger W, Recheis W. Custom implant design for large cranial defects. *Int J Comput Assist Radiol Surg*. 2016;**11**(12):2217-30. doi: 10.1007/s11548-016-1454-8. PubMed PMID: 27358081.
18. Fuessinger MA, Schwarz S, Cornelius CP, Metzger MC, Ellis E 3rd, Probst F, et al. Planning of skull reconstruction based on a statistical shape model combined with geometric morphometrics. *Int J Comput Assist Radiol Surg.* 2018;**13**(4):519-29. doi: 10.1007/s11548-017-1674-6. PubMed PMID: 29080945.
19. Liao YL, Lu CF, Sun YN, Wu CT, Lee JD, Lee ST, Wu YT. Three-dimensional reconstruction of cranial defect using active contour model and image registration. *Med Biol Eng Comput*. 2011;**49**(2):203-11. doi: 10.1007/s11517-010-0720-0. PubMed PMID: 21128121.
20. Zhang Z, Zhang R, Song Z. Skull defect reconstruction based on a new hybrid level set. *Biomed Mater Eng.* 2014;**24**(6):3343-51. doi: 10.3233/BME-141157. PubMed PMID: 25227044.
21. Qi CR, Yi L, Su H, Guibas LJ. Pointnet++: Deep hierarchical feature learning on point sets in a metric space [Internet]. arXiv [Preprint]. 2017 [cited 2017 Jun 7]. Available from: https://arxiv.org/abs/1706.02413.
22. Li J, Ellis DG, Kodym O, Rauschenbach L, Rieß C, Sure U, et al. Towards clinical applicability and computational efficiency in automatic cranial implant design: An overview of the AutoImplant 2021 cranial implant design challenge. *Med Image Anal*. 2023;**88**:102865. doi: 10.1016/j.media.2023.102865. PubMed PMID: 37331241.
23. Li J, Pepe A, Gsaxner C, Campe GV, Egger J. A baseline approach for autoimplant: the miccai 2020 cranial implant design challenge. In Workshop on clinical image-based procedures; Cham: Springer; 2020. p. 75-84.
24. Resmi S, Singh RP, Palaniappan K. Automatic skull shape completion of defective skulls using transformers for cranial implant design. *Procedia Comput Sci.* 2024;**235**:3305-14. doi: 10.1016/j.procs.2024.04.312.
25. Matzkin F, Newcombe V, Stevenson S, Khetani A, Newman T, Digby R, et al. Self-supervised skull reconstruction in brain CT images with decompressive craniectomy. In International conference on medical image computing and computer-assisted intervention; Cham: Springer; 2020. p. 390-9.
26. Matzkin F, Newcombe V, Glocker B, Ferrante E. Cranial implant design via virtual craniectomy with shape priors. In Cranial implant design challenge; Cham: Springer; 2020. p. 37-46.
27. Ellis DG, Aizenberg MR. Deep learning using augmentation via registration: 1st place solution to the AutoImplant 2020 challenge. In Cranial implant design challenge; Cham: Springer; 2020. p.

47-55.

28. Wodzinski M, Daniol M, Socha M, Hemmerling D, Stanuch M, Skalski A. Deep learning-based framework for automatic cranial defect reconstruction and implant modeling. *Comput Methods Programs Biomed.* 2022;**226**:107173. doi: 10.1016/j.cmpb.2022.107173. PubMed PMID: 36257198.
29. Xiong YT, Zeng W, Xu L, Guo JX, Liu C, Chen JT, et al. Virtual reconstruction of midfacial bone defect based on generative adversarial network. *Head Face Med.* 2022;**18**(1):19. doi: 10.1186/s13005-022-00325-2. PubMed PMID: 35761334. PubMed PMCID: PMC9235085.
30. Mainprize JG, Fishman Z, Hardisty MR. Shape completion by U-Net: An approach to the AutoImplant MICCAI cranial implant design challenge. In Cranial implant design challenge; Cham: Springer; 2020. p. 65-76.
31. Semper-Hogg W, Fuessinger MA, Schwarz S, Ellis E 3rd, Cornelius CP, Probst F, et al. Virtual reconstruction of midface defects using statistical shape models. *J Craniomaxillofac Surg.* 2017;**45**(4):461-6. doi: 10.1016/j.jcms.2016.12.020. PubMed PMID: 28202219.
32. Paszke A, Gross S, Massa F, Lerer A, Bradbury J, Chanan G, et al. Pytorch: An imperative style, high-performance deep learning library. 33rd Conference on Neural Information Processing Systems (NeurIPS 2019); Vancouver, Canada: NeurIPS Proceedings; 2019.
33. Kingma DP. Adam: A method for stochastic optimization [Internet]. arXiv [Preprint]. 2014 [cited 2014 December 22]. Available from: https://arxiv.org/abs/1412.6980.
34. Karimi D, Salcudean SE. Reducing the Hausdorff Distance in Medical Image Segmentation With Convolutional Neural Networks. *IEEE Trans Med Imaging.* 2020;**39**(2):499-513. doi: 10.1109/TMI.2019.2930068. PubMed PMID: 31329113.